NANO LETTERS

2003
Vol. 3, No. 2
163−167

Electronic Structure and Luminescence of 1.1- and 1.4-nm Silicon Nanocrystals: Oxide Shell versus Hydrogen Passivation

Zhiyong Zhou, Louis Brus,* and Richard Friesner

Chemistry Department, Columbia University, New York, New York 10027

Received November 11, 2002; Revised Manuscript Received December 8, 2002

ABSTRACT

The difference between oxide and hydrogen passivation of small Si nanocrystals is explored by all-electron, hybrid functional DFT calculations with unrestricted geometry optimization. Oxide passivation lowers the band gap by about 2.4 eV for Si_{35} cores and by about 1.5 eV for Si_{66} cores. The oxide-passivated nanocrystals have optically forbidden, indirect-gap-type transitions whereas the hydrogen-passivated nanocrystals have optically allowed, direct-gap-type transitions. The HOMO and LUMO are delocalized in both species. This result explains the experimental observation that hydrogen-passivated Si nanocrystals luminesce in the blue whereas oxide-passivated Si nanocrystals luminesce in the yellow-red.

Introduction and Methods. In this paper, we address the issue of why a small Si nanocrystal terminated with hydrogen luminesces in the blue, yet the same Si nanocrystal terminated with an oxide shell luminesces in the yellow-red. This question relates to understanding the fundamental nature and effect of nanocrystal surface passivation. In the simple quantum confinement model, the termination of broken surface bonds removes localized states from inside the band gap but does not modify the intrinsic nature of the LUMO and HOMO. We now show that the chemistry of surface termination can change the internal electronic structure. In this size regime, the oscillator strength and energy of the band gap transition can be significantly modified even if the HOMO and LUMO are delocalized over the entire nanocrystal.

Our method is all-electron DFT with an atom-centered basis and the nonlocal hybrid B3LYP functional.[1] As discussed by Kohn, Becke, and Parr, hybrid functionals are derived from the adiabatic connection formula, have the correct exchange energy in the charge density tails, and show numerical precision surpassing that of pure GGA functionals.[2] This functional was originally developed to reproduce bond energies and ionization potentials of small gas-phase molecules to within chemical accuracy (ca. 3 kcal/mol). More recently, B3LYP was shown quantitatively to reproduce the band structure and indirect gap of bulk crystalline Si and the band gaps of the complex crystalline oxides La_2CuO_4, Cr_2O_3, TiO_2, and NiO without ad hoc numerical adjustment.[3,4]

* Corresponding author. E-mail: brus@chem.columbia.edu.

10.1021/nl025890q CCC: $25.00
Published on Web 01/09/2003

As a Si nanocrystal grows in size, its physical structure and electronic properties asymptotically approach those of bulk Si, which has an indirect 1.1-eV band gap. For H passivation, there is a broad understanding of this evolution.[5−16] Larger nanocrystals show an indirect (dipole-forbidden) gap and follow quantum confinement models of band gap increase with decreasing diameter. At the smallest sizes, the band gap transition becomes allowed, at least in some species. In $Si_{35}H_{36}$ with enforced T_d symmetry, Garoufalis, Zdetsis, and Grimme[17] (hereafter GZG) calculated with B3LYP that the HOMO−LUMO transition near 4.5 eV is strongly dipole-allowed ("direct gap"). We confirm this result with full geometrical optimization. These predictions are consistent with recent evidence that some H-passivated nanocrystals in this size range do emit in the blue/UV for allowed transitions,[18−20] although definitive structural identification and spectroscopic studies have not yet appeared. Although calculations for H nanocrystals with one or several surface O atoms have recently appeared,[21−23] there have been no calculations on particles with complete oxide shells. As we shall see below, an oxide shell creates a completely different effect than a single O atom.

Although there is some variance in the experimental literature, H- and O-terminated small nanocrystals have quite different spectra and decay dynamics.[24] H-terminated nanocrystals show spectra that shift from the near-IR to the blue as size decreases. The low-temperature vibronic luminescence spectra show LO and TO Si phonons as expected for interior wave functions. In contrast, 1- to 2-nm core/shell nanocrystals, with an oxide shell made at high temperature,

Table 1. Properties of Structurally Optimized Species as Described in the Text[a]

species	$Si_{35}H_{36}$	$Si_{29}O_6(OH)_{24}$	$Si_{35}(OH)_{36}$	$Si_{66}H_{64}$	$Si_{66}O_{12}(OH)_{40}$
symmetry	T_d	D_2	T_d	T_d	C_1
HOMO	−6.81	−5.65	−5.75	−6.53	−5.56
symmetry of HOMO	T2	B1	T1	T2	A1
LUMO	−1.81	−2.77	−3.03	−2.29	−2.54
symmetry of LUMO	A1	A	A1	A1	A1
LUMO−HOMO gap	5.00	2.88	2.73	4.24	3.02
vertical ionization energy	7.73	6.64	6.68	7.50	6.36
vertical electron affinity	0.89	1.82	2.15	1.46	1.74
Fermi energy	−4.31	−4.23	−4.42	−4.48	−4.05
hardness	6.84	4.82	4.53	6.04	4.62
dipole moment (debye)	0.00	0.00	0.00	0.00	6.56

[a] All energies are in eV. $Si_{66}O_{12}(OH)_{40}$ was optimized at 3-21G level, with final energies calculated at the 6-31G* level. Other species were optimized at the 6-31G* level, with final energies calculated at the cc-pVTZ(-f) level.

show a 10^{-3} s lifetime (dipole-forbidden) yellow-red emission.[25−27] In general, oxide nanocrystals show a slowly increasing or even flat dependence of the emission wavelength on decreasing size. In an important experiment, Wolkin et al.[22] demonstrated that H-terminated nanocrystals, initially emitting above 3.0 eV in the blue, would emit near 2.0 eV in the yellow-red when oxidized. This oxidation effect is opposite of the prediction of a quantum size model because the number of elemental Si^0 atoms in the nanocrystal decreases upon surface oxidation. For the smallest sizes, low-temperature spectra show Si−O stretch vibronic structure as well as Si phonons, indicating that the wave function extends to the interface.[28]

Hydrogen Passivation and Dipole-Allowed UV Luminescence. We compare H and oxide passivation for Si_{35} and Si_{66} cores that initially are T_d fragments of the bulk lattice. Both the neutrals and anions of $Si_{35}H_{36}$ (1.1-nm diameter) and $Si_{66}H_{64}$ (1.4-nm diameter) retain T_d symmetry after complete geometrical optimization. The cations distort slightly to D_2. In Table 1, the neutral HOMO−LUMO gap in $Si_{35}H_{36}$ is 5.00 eV, in close agreement with the GZG B3LYP result for this same species[17] and slightly above the ca. 4.5-eV value given by TDLDA calculations for a similar diameter.[16] States are delocalized with no self-trapping of the extra hole or electron in the optimized positive and negative ions. The negative-ion HOMOs have similar spatial distributions to those of the neutral LUMOs.

$Si_{35}H_{36}$ is an octahedron with exposed 111 facets. Surface Si atoms have either one or two capping H atoms. The T1 HOMO has amplitude on Si−Si bonds both inside and at the center of the surface facets. The A1 LUMO has amplitude on the central Si atom and in the four surface hollows above the central surface Si atoms (see Figure 1). Yet overall, the excited state is very much on the surface with about 93% of LUMO and HOMO densities on surface Si and H atoms. In $Si_{66}H_{64}$, the wave functions begin to shift inside as expected in larger nanocrystals: 32% of the HOMO density is on the 10 interior Si atoms (see Figure 2). The LUMO has an 18% interior density, mostly inside the central tetrahedral cavity.

Unlike Si_{35}, the initial T_d Si_{66} core has two Si atoms absent at each of the six vertices where surface 111 facets intersect. Local strain is introduced when these intersections are passivated with H. In $Si_{66}H_{64}$ after structural optimization, there is an ca. 0.5-Å increase in the Si−Si spacing at these junctions because of steric repulsion between facing H atoms. Despite these local stains, $Si_{66}H_{64}$ remains T_d with a delocalized HOMO and LUMO.

In $Si_{35}H_{36}$, there are six single-electron transitions calculated within 0.21 eV of the 5.0-eV band gap, as shown in Table S1, Supporting Information. Five of the six are allowed and have radiative rates near $10^{-7} - 10^{-8}$ s. This is also true for the six single-excitation transitions that lie within 0.24 eV of the 4.24-eV gap of $Si_{66}H_{64}$. Although the exact ordering of transitions is uncertain within a few tenths of an eV, it is likely that the lowest (i.e., band gap) transition will be strongly electric-dipole-allowed (i.e., "direct gap") as predicted by GZG.

Oxide Passivation and Dipole-Forbidden Red Luminescence. We model the Si(111)/oxide interface by replacing H with hydroxyl. In $Si_{35}(OH)_{36}$, the neutrals and anions retain T_d symmetry after structural optimization, with a delocalized HOMO and LUMO and no steric strain on the surface, as in $Si_{35}H_{36}$. However, in $Si_{35}(OH)_{36}$, the band gap drops by almost a factor of 2, from 5.0 to 2.73 eV, and the HOMO symmetry changes. This difference is also present at the LDA level, which shows gaps of 3.52 and 1.21 eV for $Si_{35}H_{36}$ and $Si_{35}(OH)_{36}$, respectively, with the same basis sets and optimized geometry. Compared with $Si_{35}H_{36}$, oxide passivation strongly stabilizes the A1 LUMO with respect to other unoccupied orbitals, with 40% of the LUMO density on capping O atoms and 52% on surface Si atoms. In the triply degenerate T2 HOMO, the 75% density on surface Si bonds moves from the facet centers toward corner Si atoms that are bonded to two hydroxyl groups. The effect of oxygen termination is to draw the HOMO and LUMO toward the O atoms as compared with $Si_{35}H_{36}$ and to retard the shift of density inside with increasing size. This effect is related to the known weakening of Si−Si "back bonds" on Si atoms directly bonded to oxygen at silicon/oxide bulk interfaces. Note that the single O calculations of ref 23 also show that the localized HOMO resides on Si−Si back bonds near the oxygen.

Three optical transitions are predicted within 0.26 eV of the 2.73-eV band gap; all involve the surface A1 LUMO

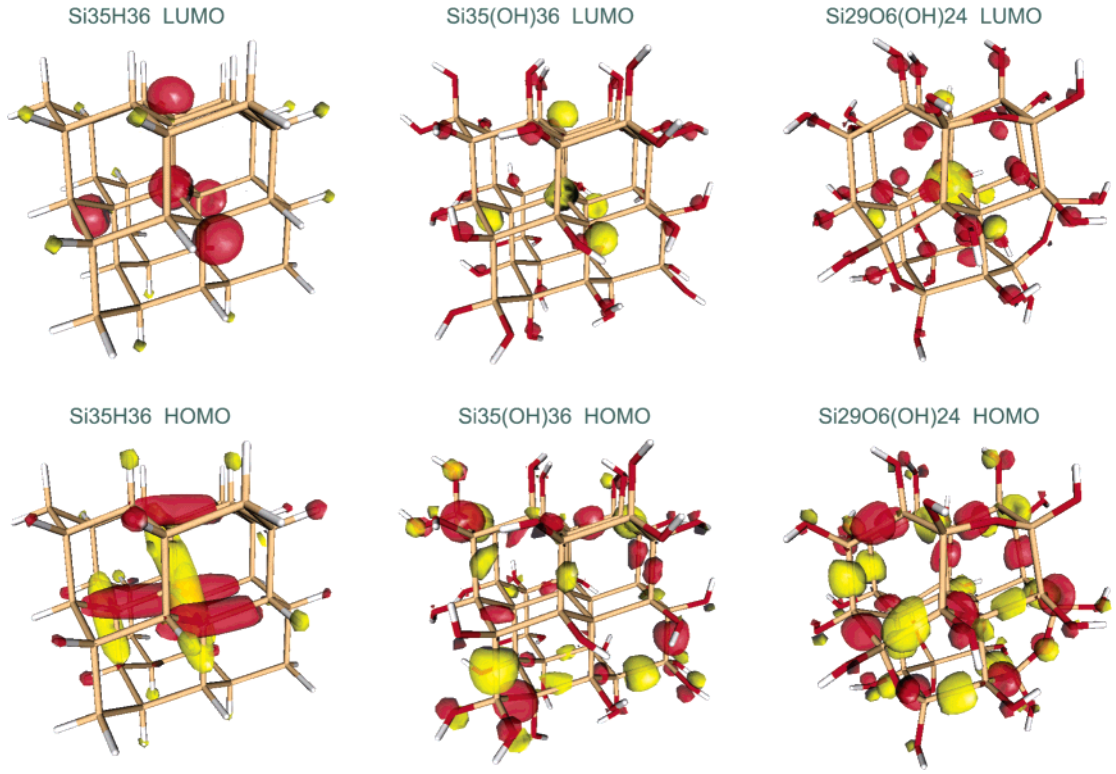

Figure 1. HOMO and LUMO for $Si_{35}H_{36}$, $Si_{35}(OH)_{36}$, and $Si_{29}O_6(OH)_{24}$. Wave function amplitude contours are at the same numerical level in all species.

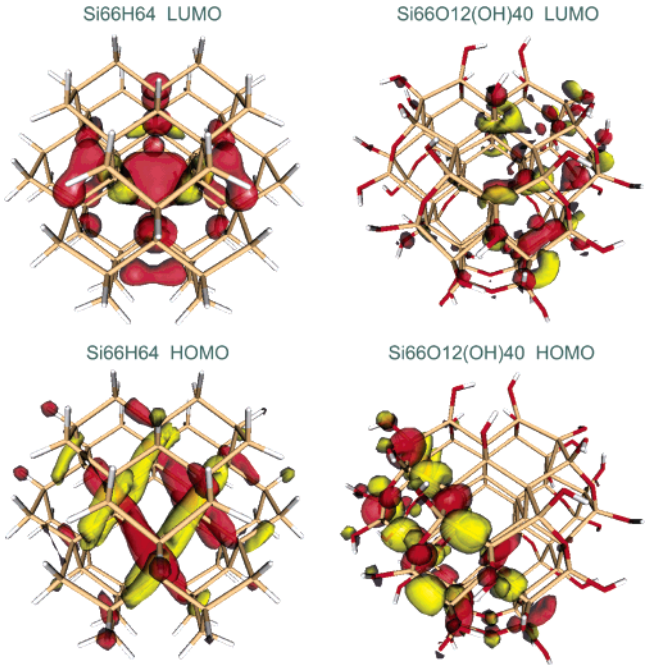

Figure 2. HOMO and LUMO for $Si_{66}H_{64}$ and $Si_{66}O_{12}(OH)_{40}$. Wave function amplitude contours are at the same numerical level in all species.

and are forbidden by symmetry. Thus, we find that oxide passivation creates a dipole-forbidden "indirect gap" like the lowest excited state, with a band gap about 2.3 eV smaller than the direct gap of H-passivated species.

$Si_{35}(OH)_{36}$ has six Si atoms at the vertices, bonded to two OH each. The frontier orbital back bonds at these corner Si atoms are susceptible to further oxidation. Thus, we also consider $Si_{29}O_6(OH)_{24}$, which has bridging O atoms replacing corner $Si(OH)_2$ groups. This change introduces some strain, and the optimized symmetry drops to D_2; the HOMO and LUMO remain delocalized. The bridged Si−Si distance at the vertices shortens to three slightly different pairs of values near 3.24 Å, as compared with 3.84 Å in bulk Si. In the LUMO, some density shifts from surface hydroxyl O atoms to the interior Si atom as compared with $Si_{35}(OH)_{36}$. In the HOMO, about 10% of the density resides on the bridging O atoms. The band gap in this strained oxide nanocrysal is close to that of $Si_{35}(OH)_{36}$. The optical transitions near the band gap should be weakly allowed, with radiative lifetimes near 10^{-5} to 10^{-6} s.

As shown in Table 1, the H and oxide species have essentially the same Fermi energy $-(I + A)/2$, where I is the ionization potential and A is the electron affinity. However, the electron-transfer hardness $(I - A)$, which is called the quasiparticle band gap in nanocrystal modeling literature, decreases by about 2 eV with oxide passivation. This result shows that the effect of oxide is not simply to create a surface dipole layer. If that were the case, then the Fermi level would become more negative and the hardness would be unchanged. Rather, oxygen has a different chemical interaction with the HOMO, which goes up in energy, and the LUMO, which goes down in energy. Electronegative oxygen increases the nanocrystal electron affinity.

All of the previous species were structurally optimized at the 6-31G* level, with energies calculated at the cc-pVTZ-(-f) level. The $Si_{66}O_{12}(OH)_{40}$ nanocrystal has OH on flat-surface 111 facets and 12 bridging O atoms at the 6

intersecting vertices. This 158-atom species tests our all-electron computational abilities; we optimize at the 3-21G level and calculate energies at the 6-31G* level. To achieve convergence, the structure is optimized in stages: we first consider $Si_{66}O_{12}H_{40}$, in which the 111 facets are H capped. This structure distorts slightly to D_2 with three different bridged Si−Si distances near 3.25 Å. Then we replace H with OH and optimize again. The final structure loses all symmetry (C_1) and shows 12 different bridged Si−Si distances from 3.229 to 3.289 Å. This species has a static dipole of 6.56 D. It is certainly possible that this species has other stable local minima.

This polar nanocrystal has electronic properties similar to those of its smaller nonpolar analogue $Si_{29}O_6(OH)_{24}$. The HOMO and LUMO are polarized to opposite sides, but the distribution over different atom types is about the same. $Si_{66}O_{12}(OH)_{40}$ has a band gap that is slightly (0.09 eV) larger than that of $Si_{29}O_6(OH)_{24}$, in direction opposition to that predicted by simple quantum confinement. The optical transitions within 0.25 eV of the band gap are calculated to be weakly allowed (10^{-4} to 10^{-6} s), again similar to those of $Si_{29}O_6(OH)_{24}$.

Discussion and Conclusions. In the 1- to 1.5-nm size regime, oxygen has a direct chemical interaction with the Si orbitals that substantially changes the HOMO and LUMO as compared with H passivation. The calculations explain the experimental results that 1- to 2-nm H-passivated nanocrystals tend to emit in the blue/violet for dipole-allowed transitions whereas core/shell oxide-passivated nanocrystals tend to emit in the yellow-red for dipole-forbidden transitions. (Note that both types of nanocrystals can have high luminescence quantum yields because the competing rates of nonradiative multiphonon relaxation are very low in the absence of structural defects.) For these sizes, the excited state is a surface excitation directly involving the capping atoms rather than a volume excitation. Kanemitsu et al. originally suggested the possibility of excited states concentrated at the interface in oxide-passivated nanocrystals.[29]

This oxide shell effect should become less important in larger species where the wave functions approach those of simple quantum confinement. We calculate band gap differences of about 2.4 eV for the Si_{35} core and about 1.5 eV for the Si_{66} core when comparing all species at the 6-31G* level, as shown in Table S2, Supporting Information. Oxide-passivated nanocrystals of 3 nm and larger experimentally seem to follow the simple quantum confinement model;[30,31] it will be interesting to examine large nanocrystals. In the transition region, the band gap may be relatively independent of size, as we see for $Si_{29}O_6(OH)_{24}$ and $Si_{66}O_{12}(OH)_{40}$. The delocalized nature of the HOMO and LUMO is insensitive to the presence of Si core strain caused by bonding to oxygen. Localized states are not observed, unlike the "trap state" of a single O atom inside the band gap of an H-passivated nanocrystal.[21−23]

Note that optically excited, oxide-passivated Si nanocrystals have been proposed as the source of the 540−960-nm "extended red emission" observed in the interstellar medium.[32−36] Our results should provide quantitative input to numerical simulations of this luminescence.

Acknowledgment. This work has been supported by the Department of Energy, Basic Energy Sciences, under contracts DE FG02-98ER14861 and DE FG02 90ER 14162. We used computational facilities that are partially supported by Columbia MRSEC grant DMR 0213574. L.B. profited from informative discussions with Mike Steigerwald and with Bob Wolkow, who suggested the connection with weakened Si−Si back bonds.

Supporting Information Available: Radiative lifetimes and oscillator strengths of the lowest transitions of species as described in the text. HOMO−LUMO gap comparison with different basis sets of structurally optimized species as described in the text. This material is available free of charge via the Internet at http://pubs.acs.org.

References

(1) Calculations were performed using Jaguar 4.0 from Schrodinger Inc.
(2) Kohn, W.; Becke, A.; Parr, R. *J. Phys. Chem.* **1996**, *100*, 12974.
(3) Muscat, J.; Wander, A.; Harrison, N. M. *Chem. Phys. Lett.* **2001**, *342*, 397.
(4) Perry, J.; Tahir-Kheli, J.; Goddard, W. A., III. *Phys. Rev. B* **2001**, *63*, 144510.
(5) Takagahara, T.; Takeda, K. *Phys. Rev. B* **1992**, *46*, 15578.
(6) Delerue, C.; Allan, G.; Lannoo, M. *Phys. Rev. B* **1993**, *48*, 11024.
(7) Delley, B.; Steigmeier, E. F. *Phys. Rev. B* **1993**, *47*, 1397.
(8) Wang, L.; Zunger, Z. *J. Phys. Chem.* **1994**, *98*, 2158.
(9) Hill, N.; Whaley, K. B. *Phys. Rev. Lett.* **1995**, *75*, 1130.
(10) Delerue, C.; Lannoo, M.; Allan, G. *Phys Rev. Lett.* **1996**, *76*, 3038.
(11) Ogut, S.; Chelikowsky, J. R.; Louie, S. G. *Phys. Rev. Lett.* **1997**, *79*, 1770.
(12) Rohlfing, M.; Louie, S. G. *Phys. Rev. Lett.* **1998**, *80*, 3320.
(13) Delerue, C.; Lannoo, M.; Allan, G. *Phys. Rev. Lett.* **2000**, *84*, 2457.
(14) Franceschetti, A.; Zunger, A. *Phys Rev. B* **2000**, *62*, 2614.
(15) Reboredo, F.; Franceschetti, A.; Zunger, A. *Phys Rev. B* **2000**, *61*, 13073.
(16) Vasiliev, I.; Ogut, S.; Chelikowsky, J. R. *Phys. Rev. Lett.* **2001**, *86*, 1813. Vasiliev, I.; Ogut, S.; Chelikowsky, J. R. *Phys. Rev. B* **2002**, *65*, 115416.
(17) Garoufalis, C.; Zdetsis, A.; Grimme, S. *Phys. Rev. Lett.* **2001**, *87*, 276402.
(18) Wilcoxon, J. P.; Samara, G. A.; Provencio, P. N. *Phys. Rev. B* **1999**, *60*, 2704.
(19) Belomoin, G.; Rogozhina, E.; Therrien, J.; Braun, P. V.; Abuhassan, L.; Nayfeh, M. H.; Wagner, L.; Mitas, L. *Phys. Rev. B* **2002**, *65*, 193406.
(20) Holmes, J. D.; Ziegler, K. J.; Doty, R. C.; Pell, L. E.; Johnston, D. P.; Korgel, B. A. *J. Am. Chem. Soc.* **2001**, *123*, 3743.
(21) Puzder, A.; Williamson, A. J.; Grossman, J. C.; Galli, G. *Phys. Rev. Lett.* **2002**, *88*, 097401.
(22) Wolkin, M. V.; Jorne, J.; Fauchet, P. M.; Allan, G.; Delerue, C. *Phys. Rev. Lett.* **1999**, *82*, 197.
(23) Vasiliev, I.; Chelikowsky, J.; Martin, R. *Phys. Rev. B* **2002**, *65*, 121302R.
(24) Shimizu-Iwayana, T.; Hole, D.; Boyd, I. *J. Phys.: Condens. Matter* **1999**, *11*, 6595.
(25) Wilson, W.; Szajowski, P.; Brus, L. *Science (Washington, D.C.)* **1993**, *262*, 1242.
(26) Brus, L. E.; Szajowski, P. F.; Wilson, W. L.; Harris, T. D.; Schuppler, S.; Citrin, P. H. *J. Am. Chem. Soc.* **1995**, *117*, 2915.
(27) Schuppler, S.; Friedman, S. L.; Marcus, M. A.; Adler, D. L.; Xie, Y. H.; Ross, F. M.; Chabal, Y. J.; Harris, T. D.; Brus, L. E.; Brown, W. L.; Chaban, E. E.; Szajowski, P. F.; Christman, S. B.; Citrin, P. H. *Phys. Rev. B* **1995**, *52*, 4910.
(28) Kanemitsu, Y.; Okamoto, S. *Phys. Rev. B* **1998**, *58*, 9652.
(29) Kanemitsu, Y.; Ogawa, T.; Shiraishi, K.; Takeda, K. *Phys. Rev. B* **1993**, *48*, 4883.
(30) Ledoux, G.; Guillois, O.; Porterat, D.; Reynaud, C.; Huisken, F.; Kohn, B.; Paillard, V. *Phys. Rev. B* **2000**, *62*, 15942.

(31) Takeoka, S.; Fujui, M.; Hayashi, S. *Phys. Rev. B* **2000**, *62*, 16820.
(32) Ledoux, G.; Ehbrecht, M.; Guillois, O.; Huisken, F.; Kohn, B.; Laguna, M. A.; Nenner, I.; Paillard, V.; Papoular, R.; Porterat, D.; Reynaud, C. *Astron. Astrophys.* **1998**, *333*, L39.
(33) Witt, A.; Gordon, K.; Furton, D. *Astrophys. J.* **1998**, *501*, L111.
(34) Darbon, S.; Zavagno, A.; Perrin, J. M.; Savine, C.; Ducci, V.; Sivan, J. P. *Astron. Astrophys.* **2000**, *364*, 723.
(35) Gordon, K. D.; Witt, A. N.; Rudy, R. J.; Puetter, R. C.; Lynch, D. K.; Mazuk, S.; Misselt, K. A.; Clayton, G. C.; Smith, T. L. *Astrophys. J.* **2000**, *544*, 859.
(36) Smith, T. L.; Witt, A. N. *Astrophys. J.* **2002**, *565*, 304.

NL025890Q